HHS Public Access

Author manuscript

J Invest Dermatol. Author manuscript; available in PMC 2018 July 01.

Published in final edited form as:

J Invest Dermatol. 2017 July ; 137(7): 1434–1444. doi:10.1016/j.jid.2017.02.983.

Compartmentation of Mitochondrial and Oxidative Metabolism in Growing Hair Follicles: A Ring of Fire

John J. Lemasters[1,2,*], **Venkat K. Ramshesh**[1], **Gregory L. Lovelace**[1], **John Lim**[3], **Graham D. Wright**[3], **Duane Harland**[4], and **Thomas L. Dawson Jr**[1,3,*]

[1]Center for Cell Death, Injury & Regeneration, Departments of Drug Discovery & Biomedical Sciences and Biochemistry & Molecular Biology, Medical University of South Carolina, Charleston, SC [2]institute of Theoretical and Experimental Biophysics, Russian Academy of Sciences, Pushchino, Russian Federation [3]Agency for Science, Technology, and Research (A*STAR), Institute for Medical Biology, Singapore [4]AgResearch NZ, Lincoln, Canterbury, New Zealand

Abstract

Little is known about the energetics of growing hair follicles, particularly in the mitochondrially abundant bulb. Here, mitochondrial and oxidative metabolism was visualized by multiphoton and light sheet microscopy in cultured bovine hair follicles and plucked human hairs. Mitochondrial membrane potential ($\Delta\Psi$), cell viability, reactive oxygen species (ROS) and secretory granules were assessed with parameter-indicating fluorophores. In growing follicles, lower bulb epithelial cells had high viability, and mitochondria were polarized. Most epithelially generated ROS co-localized with polarized mitochondria. As the imaging plane captured more central and distal cells, $\Delta\Psi$ disappeared abruptly at a transition to a non-fluorescent core continuous with the hair shaft. Approaching the transition, $\Delta\Psi$ and ROS increased, and secretory granules disappeared. ROS and $\Delta\Psi$ were strongest in a circumferential paraxial ring at putative sites for formation of the outer cortex/cuticle of the hair shaft. By contrast, polarized mitochondria in dermal papillar fibroblasts produced minimal ROS. Plucked hairs showed a similar abrupt transition of degranulation/depolarization near sites of keratin deposition, as well as a ROS-generating paraxial ‘ring of fire’. Hair movement out of the follicle appeared to occur independently of follicular bulb bioenergetics by a tractor mechanism involving the inner and outer root sheaths.

[*]Address correspondence to: John J. Lemasters, Medical University of South Carolina, DD504 Drug Discovery Building, 70 President Street, MSC 140, Charleston, SC 29425, USA, JJLemasters@musc.edu, Fax: 843-876-2353; Thomas L. Dawson, Jr, Senior Principal Investigator, Institute of Medical Biology, Agency for Science, Technology, and Research (A*STAR), 8A Biomedical Grove, #05-04 Immunos, Singapore 138648, Thomas.dawson@imb.a-star.edu.sg, Tel: +65 6407 0166.

Conflict of Interest: This work was in part funded by the Procter & Gamble Company of which TLD was an employee during initial portions of the work.

This work was substantially completed in Charleston, SC, USA and Singapore.

Introduction

On a human scalp >90% of hairs are in the growing or anagen phase (Stenn and Paus, 2001). Human scalp hairs grow 300-500 μm per day, making hair follicular epithelial cells among the body's most proliferative (Doyle and Egan, 1983, Vidali et al., 2014). In anagen hair follicles proliferation occurs in follicular epithelial cells surrounding the dermal papilla. After proliferation ceases above Auber's critical line (broadest aspect of the follicular bulb), ultrastructural, immuno-histochemical, *in-situ* hybridization and proteomic studies identify seven shells of distally migrating cell lineages that differentiate into the hair shaft and the supporting inner-root sheath (Langbein and Schweizer, 2005, Langbein et al., 2010, Legué and Nicolas, 2005, Niemann and Watt, 2002, Orwin, 1979, Plowman et al., 2015). Extension of the hair shaft is powered by a poorly understood process of cell proliferation, reshaping, and migration with narrowing of the surrounding inner root sheath, as well as deposition and hardening of keratin (Bornschlögl et al., 2016, Chapman and Gemmell, 1971, Langbein and Schweizer, 2005, Orwin and Woods, 1982, Parry et al., 2007, Plowman et al., 2015, Rafik et al., 2006, Rogers, 1964).

Measures of hair follicle metabolism using radiolabeled metabolic substrates identify glycolysis as a significant energy source, but mitochondrial metabolism also contributes (Birbeck and Mercer, 1957, Randall et al., 2003, Vidali et al., 2014, Williams et al., 1993). L-carnitine, which promotes mitochondrial β-oxidation, favorably impacts hair growth *in vitro* (Foitzik et al., 2007a) and *in vivo* (Foitzik et al., 2007b). Mitochondria are also important in follicle morphogenesis, since keratinocyte mitochondrial DNA depletion decreases hair follicle density, increases apoptosis and reduces proliferation. Moreover, stimulation of mitochondrial function with thyroid hormones prolongs anagen, increases follicular heat production, stimulates hair follicle keratinocyte proliferation and modifies intrafollicular keratin expression (Kloepper et al., 2015, Van Beek et al., 2008, Vidali et al., 2016, Vidali et al., 2014).

Previous studies characterized mitochondrial protein expression and metabolism using immunocytochemistry of fixed sections and analyses of whole follicles and whole follicle extracts. Recently, multiphoton microscopy was used to visualize stem cell migration and follicle regeneration *in vivo* (Pineda et al., 2015, Rompolas et al., 2012). Accordingly, the focus of this study was to characterize the intrafollicular distribution of mitochondrial and oxidative metabolism of anagen hair follicles in relation to secretory activity in living cultured bovine hair follicles and human hair plucks by multiphoton and light-sheet microscopy of parameter-indicating fluorophores. Our results showed striking and unanticipated gradients of mitochondrial and oxidative metabolism within different follicular regions. Specifically, a progression of mitochondrial hyperpolarization, formation of reactive oxygen species (ROS) and loss of secretory granules occurred in maturing germative epithelial cells that culminated in mitochondrial depolarization at the position of the initial formation of the hair shaft. Mitochondrial hyperpolarization and ROS formation was particularly marked in a paraxial “ring of fire” associated with formation of the hair cuticle and outer cortex.

Results

Culture of anagen bovine follicles

For our initial studies, we utilized a cultured bovine follicle model for several reasons, including difficulty of access to human follicles, lack of similarity between human and murine follicles, and new global and specifically EU regulations regarding use of animal tissue for personal care applications, which imposed restrictions from our sponsor. Bovine hair follicles were dissected from fresh cow skin obtained from local abattoirs (Randall et al., 2003). Daily photographs of dissected bovine hair follicles in culture showed the usual follicular landmarks, including the bulb, pigmented shaft and cut distal end (Fig. 1A, Day 0). A representative follicle prepared for histology showed that bulb dermal and epidermal cells were intact and surrounded by a dermal sheath (Fig. 1B). Other peripheral tissue was removed during isolation. Swelling, vacuolization and other signs of injury or death were absent. Because of curvature of the hair follicle, the companion layer and the outer root sheath were obliquely sectioned and difficult to distinguish.

Hair follicle growth was assessed daily by measurements of the lengths of the: 1) total distance from shaft tip to bulb base (including dermal tissue), 2) pigmented shaft, and 3) shaft growth beyond the cut tip (Fig. 1A, Day 7, lines 1, 2 and 3). By these measures, 25-65% of follicles grew in culture (Fig. 1C). Fig. 1A illustrates features of growth *in vitro*. Between Days 0 and 1, little hair shaft growth occurred, but between Days 1 and 4 robust growth was evident as shown by protrusion of the shaft out of the cut tip. After Day 5, the pigmented shaft continued to move outwards, but the shaft no longer increased in length. Rather, the base of the shaft moved out in parallel with its tip, and the distance between the base of the shaft and the bottom edge of the follicle increased. Fig. 1C illustrates hair shaft growth (Line 2) in relation to whole follicle length (Line 1) and hair protrusion beyond the cut edge (Line 3) for a group of follicles isolated from a single skin, confirming that shaft protrusion beyond the cut edge often continued after hair shaft elongation ceased, especially after Day 3 or 4. In still other follicles, neither hair shaft elongation nor shaft movement away from the bulb occurred. Other than via hair shaft movement and elongation, anagen, catagen and non-growing follicles could generally not be distinguished based on initial appearance.

Characterization of cell viability and mitochondrial metabolism in bovine follicles

Follicles observed to be growing after 1 day were incubated with propidium iodide (PI) to label nonviable cell nuclei and rhodamine 123 (Rh123) to visualize mitochondrial membrane potential ($\Delta\Psi$) (Zahrebelski et al., 1995). These and other fluorophores did not prevent hair growth. Many dermal sheath cells contained Pi-labeled nuclei and did not label with Rh123, signifying loss of viability (Fig. 2A). PI labeling was variable between samples and sometimes patchy. Nearly all epithelial cells inside the dermal sheath excluded PI and were strongly labeled by Rh123. Occasionally, an epithelial matrix or outer root sheath cell labeled with PI but not Rh123, indicating PI was crossing the basement membrane to label nonviable cells (Figure 2B, asterisk). Rh123 staining was strong near the follicle base. Distal to the germative matrix cells and about 50-100 μm from the base of the bulb, complete loss of Rh123 fluorescence occurred abruptly (Fig. 2A-C). Beyond this transition, images were

nearly black except for a fringe of punctate chemiluminescence from melanin granules. Melanin chemiluminescence was lost moving more distally into the hair. Suppl. Movie 1 shows a 5-μm increment through-focus 120-μm Z-stack of a PI and Rh123-labeled hair bulb viewed from its side, which further illustrates loss of viability of dermal cells, robust uptake of Rh123 by follicular epithelial cells and abrupt mitochondrial depolarization moving outwards from the follicular bulb.

Distally, fluorescence disappeared in a dark region often punctuated with bright chemiluminescent spots, typical of melanin granules. This black region represented the initial formation of the hair shaft matrix and continued distally to the emergence of the hair shaft at the follicle apex (not shown). Melanin chemiluminescence clearly indicated that excitation wavelengths penetrated to the center of the hair matrix and that the lack of signals from fluorophores indicated a lack of staining.

A metabolic transition zone defined by secretory granules and increased mitochondrial ΔΨ

Bovine hair follicles were labelled with Rh123 and lysotracker red (LTR), the latter to label acidic compartments of lysosomes, endosomes and many types of secretory vesicles (Kujpers et al., 1989, Moreno et al., 2010). LTR intensely stained some cells in the dermal sheath but generally not dermal cells directly adjacent to the follicular bulb (Fig. 2C). Epithelial cells in the follicle interior also contained LTR-labeled vesicles (Fig. 2C and D). Epithelial cell vesicle labeling by LTR was less intense than in the dermis. Inside follicles, individual LTR labelled vesicles were evident within epithelial cells (Figure 2D). The image in Fig. 2D was rescaled to amplify red fluorescence; hence Rh 123-labeled mitochondria appeared green-yellow in the overlay due to bleed-through of some Rh123 fluorescence into the red channel. By contrast, LTR-labeled vesicles displayed pure red fluorescence. Notably, these red-staining granules were lost in parallel with mitochondrial depolarization (loss of yellow-green Rh123 fluorescence) at the major transition further distal into the follicle interior (Fig. 2D). Beyond the transition of mitochondrial depolarization, only scattered yellow melanin granules in the black hair matrix were observed (Fig. 2D). Despite the abrupt loss of mitochondrial polarization and loss of vesicles, nuclear labeling by PI remained absent.

Localization of reactive oxygen species generation

Growing follicles were co-loaded with chloromethyldihydrodichlorofluorescein (cmH_2DCF, ester-loaded as cmH_2DCF-diacetate), a green-fluorescing hydroperoxide indicator, and tetramethylrhodamine methylester (TMRM), a red-fluorescing ΔΨ indicator, to reveal ROS generation in comparison to mitochondrial polarization (Cathcart et al., 1983, Kim et al., 2012). In a representative paraxial longitudinal section 45μm into the follicle, dermal cells adherent to the surface of the follicular bulb showed the strongest labeling with green cmDCF fluorescence (Fig. 3A, single arrow). Green cmDCF fluorescence was generally weaker within follicular epithelial cells and consistently co-localized with TMRM-labeled polarized mitochondria, making mitochondria appear yellow-orange in the overlays. In longitudinal image sections, clefts of non-fluorescent material projected downwards from the hair shaft into the follicular bulb under a single layer of epithelial cells below the follicle surface and just distal to the widest part of the bulb (Fig. 3A, asterisks). Notably, cells

labeling strongly with both cmDCF and TMRM were present at the proximal (basal) apex of these non-fluorescent clefts (Fig. 3A, double arrows). Although abundant in the central cortical region of the newly formed hair matrix, chemiluminescent melanin granules (yellow-green puncta in an otherwise black hair matrix) were absent in clefts. Which cell line or lines constitute the cells strongly labeled cmDCF and TMRM is not clear, but the lack of melanin granules in the non-fluorescent clefts above (distal) to these cells suggests that these cells are not forming the hair cortex.

Three-dimensional reconstructions showed that strongly cmDCF and TMRM-labeled cells formed strands crisscrossing the dermal sheath (Fig. 3, Suppl, Movies 2 and 3), which were likely blood vessels (Hordinsky and Ericson, 2008). In favorable projections inside the follicular bulb, brightly cmDCF and TMRM-labeled cells lined the proximal apices of the dark clefts. These highly polarized ROS-generating cells formed a circumferential ring within the follicle (Fig. 3B, arrows; Suppl. Movies 2 and 3). Individual cells or groups of cells in the ring appeared to be separated one from another by dark, poorly fluorescent areas, and various of these cells stained intensely for $\Delta\Psi$ alone, ROS alone or both $\Delta\Psi$ and ROS.

Bovine hair follicles double-stained with Rh123 plus LTR or TMRM plus cmH_2DCF showed variations of mitochondrial polarization (Fig. 2 and 3). At the primary center of cortical hair matrix deposition, greater $\Delta\Psi$ was typically noted immediately proximal to the sharp transition of depolarization and initial keratinization (Fig. 4A and B, asterisks). Even stronger hyperpolarization, and therefore an even more stark transition, occurred at the apex of the paraxial ring (Fig. 3A, double arrows). Moreover, as hyperpolarization occurred, loss of LTR-labeled granules took place in parallel across the base of the newly forming hair shaft and thus involved several different cell lineages (Fig. 4A).

Dermal papilla

Bovine dermal papillae penetrated the follicular bulb obliquely from the side rather than the middle, as is usually depicted for human follicles but consistent with the “curved” dermal papillae of fine-wool sheep (Fig. 4C) (Auber, 1952). Three-dimensional renderings confirmed that dermal papillae penetrated the bulb obliquely (see Suppl. Movies 4 and 5).

In TMRM and cmDCF-labeled follicles, dermal papilla cells displayed polarized mitochondria, but TMRM intensity was much less than nearby epidermal cells. The nearly pure red color of mitochondria in dermal papilla cells signified little mitochondrial ROS generation. By contrast, the orange color in the overlay of green and red fluorescence of mitochondria in germative matrix cells documented $\Delta\Psi$ as well ROS generation (Fig. 4C).

Growing versus non-growing bovine follicles

Variability was observed in the growth of cultured bovine follicles. Some paused growth for one or two days and then spontaneously began growth (see Fig. 1C), whereas others never grew. Viable germative matrix cells of growing follicles contained robustly polarized mitochondria filling the base of the follicular bulb (Fig. 2-4). In at least some non-growing hair follicles, viable bulb germative matrix epithelial cells with polarized mitochondria were greatly diminished (Fig. 4D). ROS generation assessed by cmDCF fluorescence was also

minimal. In these follicles, elongation of the hair shaft ceased, and the proximal end of the hair fiber began to move out of the follicle bulb (see Fig. 1).

Human hair plucks confirm bovine findings

Melanin-free temporal hairs were plucked from two human subjects (JJL and TLD) and labeled with Rh123 and LTR. Moving distally from the base, differentiating germative matrix epithelial cells developed distinct LTR-labeled vesicles (Fig.5A, inset, Zone 1). Then in sequence as the cells moved outward, mitochondria hyperpolarized (Zone 2), lysosomal vesicles disappeared, (Zone 3), and then mitochondria abruptly depolarized (Zone 4). In particular, loss of lysosomal vesicles again appeared to occur one or two cell layers deep from the transition to mitochondrial depolarization (Fig. 5A, inset).

Plucked human hairs were also labeled with tetramethylrhodamine ethylester (TMRE, $\Delta\Psi$-indicating fluorophore similar to TMRM) and cmDCF for imaging by light sheet microscopy. Multiple slices through the entire hair were reconstructed in 3-dimensions. Although lateral resolution was lower than multiphoton microscopy and individual mitochondria could not be resolved, side and top projections clearly showed a ring of intense cmDCF and TMRE fluorescence (yellow or yellow-green in the overlay) inside of the bulb of the plucked hairs above their base (Fig. 5B, Suppl. Movie 6). Note that the lateral brightness gradient was an artifact created by absorbance and scattering of the illuminating light sheet as it passed through the specimen.

Discussion

Bovine hair follicles as a model of follicular growth and differentiation

The difficulty of obtaining human follicles and the difference between human and murine follicles necessitates development of new model systems. Bovine follicles are available, meet many global animal use regulations, and more closely resemble human follicles. In this study we confirmed that cultured bovine hair follicles maintained a histology comparable to that of normal, intact human hair follicles. Overall, dissected individual bovine hair follicles grew variably in culture, often with hair shaft elongation characteristic of human anagen. In others, the hair shaft began to move away from the follicular bulb without elongating, a characteristic of catagen (Philpott et al., 1990). Some growth variation was seasonal with less growth in winter months, as reported previously in both bovine and human hair (Dowling, 1958, Kunz et al., 2009, Randall and Ebling, 1991). Overall during days 1-4 of culture, many hairs grew as in anagen, whereas afterwards growth resembled catagen. The fluorophores used did not prevent continued hair growth.

Through-focus images (*z*-stacks) collected beginning at the bottom of the bulb with the hair follicle standing on end showed that the dermal papilla penetrated the base of the bulb obliquely from the side rather than from the bottom, as is usually depicted for human follicles. Oblique entry is consistent with the “curved” dermal papillae of fine-wool sheep (Fig. 4C, Suppl. Movies 4 and 5) (Auber, 1952). Notably, the dermal papillae directly abutted two different structures: 1) the TMRM- and cmDCF-labeled germative matrix epithelial cells and 2) the newly formed and melanin-containing hair matrix beyond the

transition zone where TMRM and cmDCF fluorescence was excluded. This anatomic arrangement likely facilitates exchange of growth and other signals between dermal papillae and both the matrix epithelial cells and the newly formed hair matrix (Fig. 4C).

Compartmentalization of metabolism in the follicle matrix

Many dermal sheath cells were non-viable in discrete patches, suggesting that mechanical manipulations (forceps, *etc.*) may have contributed to damage. By contrast, nearly all matrix and outer root sheet cells inside the dermal sheath were viable: they had high $\Delta\Psi$ and excluded PI despite demonstrable dye penetration (Figure 2B, asterisk). When most cells at the base of the hair bulb retained viability and $\Delta\Psi$, hair growth occurred notwithstanding variable and sometimes substantial loss of dermal sheath cell viability. The high $\Delta\Psi$ near the follicle base corresponded to proliferating and differentiating germative matrix epithelial cells.

These observations demonstrated that germative matrix epithelial cells at the base of the bulb of growing follicles were viable and contained abundant, metabolically active mitochondria, extending prior work showing the presence and metabolism of mitochondria by morphometry, immunohistochemistry and heat generation (Kloepper et al., 2015, Vidali et al., 2014). These measurements of mitochondrial function by multiphoton and light sheet microscopy have the advantage of much improved temporal resolution compared to protein expression, immunocytochemistry, enzyme activity and DNA content, which may persist long after cessation of the metabolism of interest.

As matrix cells differentiated and moved upwards (distally), a major transition developed where all $\Delta\Psi$ was abruptly lost (Fig. 2A and B). Although the cells were now non-viable by metabolic measures, PI staining was absent. Either PI could not penetrate beyond the transition, or nuclear DNA had become degraded and PI had no place to bind into a clearly defined nuclear structure. The latter possibility is supported by studies showing that nuclei and DNA in differentiating epithelial germative matrix cells become progressively degraded after cell division ceases above Auber's critical line (Downes et al., 1966, Montagna and Parakkal, 1974, Orwin, 1969, Swift, 1977), even as differentiation proceeds with apparent expression of new keratins and keratin-associated proteins (Langbein and Schweizer, 2005, Langbein et al., 2010, Plowman et al., 2015). Similar degradation of nuclear structure and DNA occurs in the stratum lucidum/corneum of skin (Broekaert et al., 1986, Fuchs, 1990).

A major metabolic transition during hair shaft formation

Bovine hair follicles stained with the $\Delta\Psi$ indicators, Rh123 and TMRM, showed gradients of mitochondrial $\Delta\Psi$ as the primary center of cortical hair matrix deposition was approached (Fig. 2-4). Specifically, $\Delta\Psi$ became greatest immediately proximal to the sharp transition of depolarization and initial keratinization. Measurements of background-subtracted pixel intensities showed an up to 130% increase in Rh123 fluorescence as the sharp transition was approached compared to germinal epithelial cells deeper in the follicle (Fig. 2C).

To assess whether loss of lysosomal vesicles occurred in parallel with loss of $\Delta\Psi$, follicles were co-labeled with Rh123 ($\Delta\Psi$) and LTR (lysosomes, endosomes and many types of secretory granules) (Kujpers et al., 1989, Moreno et al., 2010). LTR intensely stained some

dermal sheath cells (Fig. 2C). Their identity is unknown, but some could represent reactive macrophages that have a high content of lysosomes and are known to inhabit this area (Parakkal, 1969). Epithelial cells in the follicle interior also contained vesicles labeled with LTR, but the intensity of staining was less than in the dermis (Fig. 2C and D). This suggests that the vesicles in the follicle interior were less acidic than the LTR-labeled structures, presumably lysosomes, in dermal cells.

LTR labeling of intrafollicular epithelial vesicles disappeared in parallel with mitochondrial depolarization (loss of yellow-green Rh123 fluorescence) at the major transition further into the follicle interior. Thus, loss of LTR-positive vesicles and mitochondrial depolarization took place coordinately with LTR vesicle loss occurring slightly in advance of mitochondrial depolarization as differentiating germative matrix cells matured and moved outwards and inwards (Fig. 2D). After this loss of LTR-labeled vesicles and $\Delta\Psi$, only scattered yellow melanin granules in the black hair matrix could be visualized. Overall, these results indicated a loss of living cell function and a transition into mainly structural material lacking conventional metabolic activity. Therefore, the major transition of mitochondrial depolarization was likely analogous to the abrupt junction between the stratum granulosum and stratum lucidum/corneum of skin (Fuchs, 1990). At this junction, keratohyalin granules are released, the plasma membrane permeability barrier is lost, and further new structural changes occur, such as crosslinking of keratins and keratin-associated proteins.

Reactive oxygen species generation reveals a “ring of fire”

Deposition of keratins and functional cross-linking require a highly oxidative environment, including generation of reactive oxygen species (ROS) that also attack lipids and cause lipid peroxidation (Repetto et al., 2012). Thus, we co-labeled growing follicles with cmH_2DCF, a green-fluorescing hydroperoxide indicator, and TMRM, a red-fluorescing $\Delta\Psi$ indicator, to reveal ROS generation in comparison to mitochondrial polarization (Cathcart et al., 1983, Kim et al., 2012).

Inside the follicle, ROS generation co-localized with mitochondrial $\Delta\Psi$ and increased in parallel with $\Delta\Psi$ as the transition zone of complete mitochondrial depolarization was approached (Fig. 3A and 4C). In favorable projections inside the follicular bulb, cells with both high ROS generation and high $\Delta\Psi$ lined the proximal apices of paraxial secondary hair-forming clefts (Fig. 3A, double arrows), forming a circumferential ring within the follicle (Fig.3B, arrows; Suppl. Movies 2 and 3). One possibility for this pattern is that mitochondrial hyperpolarization (TMRM alone) led to mitochondrial ROS generation (TMRM plus cmDCF), followed by mitochondrial dysfunction and depolarization (cmDCF alone), but future studies will be required to determine the exact temporal and mechanistic sequence of the events and their role in hair follicle cycling. We name this structure a ‘ring of fire’, where mitochondrial hyperpolarization is the heat and ROS generation the fire.

Dermal papilla cells are less metabolically active than epidermal cells

In TMRM and cmDCF-labeled follicles, dermal papilla cells displayed polarized mitochondria, but the intensity was much less than in nearby epidermal cells. The nearly pure red color of dermal papilla mitochondria signified high $\Delta\Psi$ but little ROS generation.

By contrast, the orange mitochondria in the overlay of green and red fluorescence in epidermal matrix cells documented mitochondrial $\Delta\Psi$ plus ROS generation (Fig. 4C). Thus, epidermal bulb cells showed greater mitochondrial and oxidative metabolism compared to dermal papilla cells.

Growing versus non-growing bovine follicles

Cultured bovine follicles showed variability in growth vs. non-growth (Fig. 1), and some non-growing follicles showed dramatic differences in comparison to growing follicles. Specifically, some non-growing follicles showed only a thin layer of viable, more weakly polarized epithelial germative matrix cells at the very base of the follicular bulb (Fig. 4D). This change appeared to represent movement of the transition zone of mitochondrial depolarization to cells close to or resting on the basement membrane, reflecting a paucity of proliferating and differentiating germative matrix cells and hence lack of hair formation. ROS generation was minimal, further evidence of decreased oxidative metabolism (Fig. 4D). By contrast in growing follicles, viable germative matrix epithelial cells with robustly polarized mitochondria filled the base of the follicular bulb (Fig. 2-4). This increased mitochondrial metabolism may account for increased heat production by hair follicles in prolonged anagen, as observed after thyroid hormone stimulation (Kloepper et al., 2015, Van Beek et al., 2008, Vidali et al., 2016, Vidali et al., 2014). Presumably in fully functional follicles, proliferation of matrix epidermal cells kept pace with the outward movement of the hair shaft, which allowed the position of the follicular bulb in the dermis to remain stable. In at least some non-growing follicles, viable bulb epithelial cells with polarized mitochondria were greatly diminished, and the follicular bulb began to move towards the surface, evidently because proliferation could no longer keep pace with hair shaft movement out of the follicle. The most parsimonious explanation is that individual hairs were not being “pushed” out solely by cell division. Rather, a tractor mechanism appeared to be pulling hair shafts towards the skin surface. Tractor force was likely generated at one or both of the interfaces between the companion layer and the outer root sheath or the hardened Henle's layer via well-developed desmosomes and connected cytoskeleton, as observed in human, rodent and wool follicles (Ito, 1986, Langbein et al., 2002, Morioka, 2005, Orwin, 1971). A tractor mechanism allows for both outward movement of hair fibers and strong adherence within the skin. The force required to extract (pluck) human hairs is proportional to the diameter and depth of the follicle, as well as the stage of growth (anagen/catagen/telogen), consistent with an adhering tractor mechanism (El-Rifaie et al., 2015).

Human hair plucks confirm bovine findings

To characterize metabolic activity in human hairs, melanin-free temporal hairs were plucked from human subjects, labeled with Rh123 and LTR, and imaged with light sheet microscopy. Plucked hairs typically break across the bulb near its distal end and separate laterally along the companion layer, although parts of the outer root sheath are sometimes included. Plucks do not include the dermal papilla or germative matrix cells at early stages of differentiation (Bassukas and Hornstein, 1989, Langbein et al., 2002) (see Fig. 6). Nonetheless, moving out from the broken base of plucked hairs, differentiating epithelial cells developed distinct LTR-labeled vesicles (Fig. 5A, inset, Zone 1), followed in sequence by mitochondrial hyperpolarization (Zone 2), loss of the LTR-labeled vesicles (Zone 3) and mitochondrial

depolarization (Zone 4). In particular, loss of LTR-labeled vesicles again appeared to occur one or two cell layers deep from the transition to mitochondrial depolarization (Fig. 5A, inset).

Human hair plucks were also labeled with TMRE and cmDCF to visualize ΔΨ and ROS by light sheet microscopy. Projections clearly showed the ring of intense cmDCF and TMRE fluorescence (yellow or yellow-green in the overlay) inside of the bulb of the plucked hairs above the base (Fig. 5B, Suppl. Movie 6). Similar to our observations by multiphoton microscopy in bovine hair follicles, the ring was discontinuous even on its brightest side. (compare to Fig. 3B). Thus, plucked human hairs confirmed the findings in bovine hair follicles that 1) LTR labeled vesicle loss, mitochondrial hyperpolarization, and enhanced ROS generation occurred in differentiating epidermal matrix cells as the abrupt transition of mitochondrial depolarization was approached and 2) mitochondrial hyperpolarization and ROS generation were even greater in a ‘ring of fire’ associated with formation of the outer layers of the hair shaft, including the cuticle and possibly the outer cortex or Henle's layer. However, future studies will be needed to determine the specific cell lineages associated with the ring of fire and the ring's relation to established morphological landmarks of hair development (*e.g.*, hardening of Henle's layer).

The multiphoton and light sheet microscopic studies described here are the first to our knowledge to characterize the compartmentation of hair follicle metabolic activity, here modelled with isolated bovine hair follicles and confirmed in plucked human hairs. The results showed robust mitochondrial metabolism and a progression of mitochondrial hyperpolarization, ROS generation, loss of secretory vesicles and subsequent mitochondrial depolarization at the interface between viable matrix epidermal cells and the newly forming hair shaft, as illustrated schematically in Fig. 6. In particular, cuticular/outer cortical hair formation occurred in a highly oxidative ‘ring of fire’ of exaggerated mitochondrial hyperpolarization and ROS generation. These observations support the conclusion that ROS generation is an integral event in hair formation, which promotes the oxidative environment needed for cross-linking of keratins and other hair matrix proteins, rather than a toxic by-product of mitochondrial metabolism. The results also showed that differentiating germative matrix epithelial cells abruptly lost metabolic activity and became non-viable as they transformed into hair shaft matrix. We hypothesize this transformation is analogous to the stratum granulosum-stratum lucidum/corneum transition in skin. The similarity of the findings in both isolated bovine follicles and plucked human hair suggests that these events reflect native physiology and are likely to occur in most mammalian hair follicles. Future work with human follicles will be necessary to better characterize the mechanisms underlying these events and to develop interventions to improve hair quality and growth. Better understanding of the mechanisms underlying hair growth should also lead to better strategies to treat alopecia and hirsutism, enhance agricultural fiber production and develop new cosmetic products.

Materials And Methods

Bovine hair follicles

Single follicles were dissected from bovine flank, trimmed apically below the sebaceous gland and cultured in modified Williams E medium at 37°C in 5% CO_2/air, as described (Philpott et al., 1994). Follicles were fixed in phosphate-buffered 2% formaldehyde, paraffin embedded, and stained with hematoxylin and eosin.

Multiphoton imaging

Bovine follicles cultured as above were incubated overnight with various combinations of a red-fluorescing dye – 1 μM LTR, 30 μM PI or 1 μM TMRM – and a green-fluorescing dye − 1 μM Rh123 or 20 μM cmH_2DCF-DA (Thermo Fisher Scientific). During imaging, a small nylon screen was placed over the follicle to minimize motion artifacts. The fluorescence of PI and Rh123 was collected using 800-nm multiphoton excitation (6-8% laser power) from a Coherent Chameleon Ultra II Ti-Sapphire pulsed laser with a Zeiss LSM 510 NLO inverted laser scanning confocal/multiphoton microscope by a 40×, NA 1.2 water-immersion objective. The fluorescence of TMRM and cmDCF was collected using 820-nm multiphoton excitation (12% power). The plane of imaging was 45 μm from the lateral follicle surface unless otherwise specified.

Human Hair Plucks

Minimally pigmented human hairs were plucked from the temporal scalp and cultured as above. Plucked hairs were imaged by multiphoton microscopy after loading with cmDCF and TMRM, as described above except using a MaiTai HP DeepSee laser, an Olympus FV1200 mulitphoton microscope and a 30× 1.05 NA silicone oil immersion objective lens. Plucked human hairs were also imaged after overnight loading using a light sheet microscope built at the Institute of Medical Biology in Singapore with excitation from 488-nm and 561-nm Coherent OBIS lasers, emission through 525±25 nm and 641±37.5 nm band pass filters, and an Olympus 20× NA. 1.0 water dipping objective. TMRE (1 μM) replaced TMRM. Full width half maximal at the thinnest portion of the light sheet was 5 μm Images are representative of three or more experiments. Human hair plucks were acquired under the approval of the National University of Singapore Institutional Review Board approval number B-15-236 with written informed consent.

Supplementary Material

Refer to Web version on PubMed Central for supplementary material.

Acknowledgments

This work was supported by a contract from the Procter & Gamble Company to Medical University of South Carolina and by A*STAR, Singapore. Imaging facilities were supported, in part, by P30 CA138313 and 5 P20 GM103542-03 from the National Institutes of Health. We thank Ben Hulette for dissection of bovine hair follicles and Dr. Sohail Ahmed expert advice on light sheet microscopy.

References

Auber L. VII.—The Anatomy of Follicles Producing Wool-Fibres, with special reference to Keratinization. Earth and Environmental Science Transactions of the Royal Society of Edinburgh. 1952; 62:191–254.

Bassukas ID, Hornstein OP. Effects of plucking on the anatomy of the anagen hair bulb. Archives of dermatological research. 1989; 281:188–92. [PubMed: 2774646]

Birbeck MSC, Mercer EH. Electron Microscopy of the human hair follicle. Journal of Biophysical and Biochemical Cytology. 1957; 3:203–14. [PubMed: 13438903]

Bornschlögl T, Bildstein L, Thibaut S, Santoprete R, Fiat F, Luengo GS, et al. Keratin network modifications lead to the mechanical stiffening of the hair follicle fiber. Proceedings of the National Academy of Sciences. 2016:201520302.

Broekaert D, Van Oostveldt P, Coucke P, De Bersaques J, Gillis E, Reyniers P. Nuclear differentiation and ultimate fate during epidermal keratinization. Archives of Dermatological Research. 1986; 279:100–11. [PubMed: 2436581]

Cathcart R, Schwiers E, Ames BN. Detection of picomole levels of lipid hydroperoxides using a dichlorofluorescein fluorescent assay. Analytical Biochemistry. 1983; 134:111–6. [PubMed: 6660480]

Chapman RE, Gemmell RT. Stages in the formation and keratinization of the cortex of the wool fiber. Journal of Ultrastructure Research. 1971; 36:342–54. [PubMed: 4938267]

Dowling DF. Seasonal changes in coat characters in cattle. Proceedings of the Australian Society of Animal Production. 1958:69–80.

Downes AM, Chapman RE, Till AR, Wilson PA. Proliferative Cycle and Fate of Cell Nuclei in Wool Follicles. Nature. 1966; 212:477–9.

Doyle PT, Egan JK. The utilization of nitrogen and sulfur by weaner and mature merino sheep. Australian Journal of Agricultural Research. 1983; 34:433–9.

El-Rifaie AA, Abdel Wehab AM, Gohary Y, El-Rifaie AE. The trichotillometry: a technique for hair assessment. Skin Research and Technology. 2015:n/a–n/a.

Foitzik K, Hoting E, Förster T, Pertile P, Paus R. L-Carnitine-L-tartrate promotes human hair growth in vitro. Experimental Dermatology. 2007a; 16:936–45. [PubMed: 17927577]

Foitzik K, Hoting E, Heinrich U, Tronnier H, Paus R. Indications that topical l-carnitin-l-tartrate promotes human hair growth in vivo. Journal of Dermatological Science. 2007b; 48:141–4. [PubMed: 17804203]

Fuchs E. Epidermal Differentiation: The Bare Essentials. 1990; 111:2807–14.

Hordinsky, M., Ericson, M. Hair Follicle Vascularization and Innervation. In: Blume-Peytavi, U.Tosti, A., Trüeb, RM., editors. Hair Growth and Disorders SE - 5. Springer; Berlin Heidelberg: 2008. p. 75-83.

Ito M. The innermost cell layer of the outer root sheath in anagen hair follicle: light and electron microscopic study. Archives of dermatological research. 1986; 279:112–9. [PubMed: 2436582]

Kim JS, Wang JH, Lemasters JJ. Mitochondrial permeability transition in rat hepatocytes after anoxia/reoxygenation: role of Ca2+-dependent mitochondrial formation of reactive oxygen species. American journal of physiology Gastrointestinal and liver physiology. 2012; 302:G723–31. [PubMed: 22241863]

Kloepper JE, Baris OR, Reuter K, Kobayashi K, Weiland D, Vidali S, et al. Mitochondrial Function in Murine Skin Epithelium Is Crucial for Hair Follicle Morphogenesis and Epithelial–Mesenchymal Interactions. Journal of Investigative Dermatology. 2015; 135:679–89. [PubMed: 25371971]

Kujpers GA, Rosario LM, Ornberg RL. Role of intracellular pH in secretion from adrenal medulla chromaffine cells. Jbc. 1989; 264:698–705.

Kunz M, Seifert B, Trüeb RM. Seasonality of hair shedding in healthy women complaining of hair loss. Dermatology. 2009; 219:105–10. [PubMed: 19407435]

Langbein L, Rogers MA, Praetzel S, Aoki N, Winter H, Schweizer J. A novel epithelial keratin, hK6irs1, is expressed differentially in all layers of the inner root sheath, including specialized

Huxley cells (Flügelzellen) of the human hair follicle. Journal of investigative dermatology. 2002; 118:789–99. [PubMed: 11982755]

Langbein, L., Schweizer, J. Keratins of the Human Hair Follicle1. Cytology BT-IRo. , editor. Academic Press; 2005. p. 1-78.

Langbein L, Yoshida H, Praetzel-Wunder S, Parry Da, Schweizer J. The keratins of the human beard hair medulla: the riddle in the middle. The Journal of investigative dermatology. 2010; 130:55–73. [PubMed: 19587698]

Legué E, Nicolas JF. Hair follicle renewal: organization of stem cells in the matrix and the role of stereotyped lineages and behaviors. Development. 2005; 132:4143–54. [PubMed: 16107474]

Montagna W, Parakkal PF. Structure and Function of Skin. 1974

Moreno A, SantoDomingo J, Fonteriz RI, Lobaton CD, Montero M, Alvarez J. A confocal study on the visualization of chromaffin cell secretory vesicles with fluorescent targeted probes and acidic dyes. Journal of Structural Biology. 2010; 172:261–9. [PubMed: 20600953]

Morioka K. Hair follicle, differentiation under the electron microscope - an atlas. 2005

Niemann C, Watt FM. Designer skin: lineage commitment in postnatal epidermis. Trends in Cell Biology. 2002; 12:185–92. [PubMed: 11978538]

Orwin DFG. New Ultrastructural Features in the Wool Follicle. Nature. 1969; 223:401–3. [PubMed: 4980853]

Orwin DFG. Cell Differentiation in the Lower Outer Sheath of the Romney Wool Follicle: A Companion Cell Layer. Australian Journal of Biological Sciences. 1971; 24:989–1000. [PubMed: 5159202]

Orwin DFG. The cytology and cytochemistry of the wool follicle [Includes fiber development and properties]. International review of cytology. 1979

Orwin DFG, Woods JL. Number changes and development potential of wool follicle cells in the early stages of fiber differentiation. Journal of Ultrastructure Research. 1982; 80:312–22. [PubMed: 7131649]

Parakkal PF. Role of macrophages in collagen resorption during hair growth cycle. Journal of Ultrastructure Research. 1969; 29:210–7. [PubMed: 5362393]

Parry DAD, Strelkov SV, Burkhard P, Aebi U, Herrmann H. Towards a molecular description of intermediate filament structure and assembly. Experimental cell research. 2007; 313:2204–16. [PubMed: 17521629]

Philpott MP, Green MR, Kealey T. Human hair growth in vitro. Journal of cell science. 1990; 97(Pt 3): 463–71. [PubMed: 1705941]

Philpott MP, Sandersa D, Westgateb GE, Kealey T. Human hair growth in vitro : a model for the study of hair follicle biology. 1994; 7

Pineda CM, Park S, Mesa KR, Wolfel M, Gonzalez DG, Haberman AM, et al. Intravital imaging of hair follicle regeneration in the mouse. Nature protocols. 2015; 10:1116–30. [PubMed: 26110716]

Plowman JE, Harland DP, Ganeshan S, Woods JL, van Shaijik B, Deb-Choudhury S, et al. The proteomics of wool fibre morphogenesis. Journal of Structural Biology. 2015; 191:341–51. [PubMed: 26208467]

Rafik ME, Briki F, Burghammer M, Doucet J. In vivo formation steps of the hard alpha-keratin intermediate filament along a hair follicle: evidence for structural polymorphism. Journal of structural biology. 2006; 154:79–88. [PubMed: 16458019]

Randall, Va, Ebling, FJG. Seasonal changes in human hair growth. Brisith Journal of Dermatology. 1991; 124:146–51.

Randall, Va, Sundberg, JP., Philpott, MP. Animal and in vitro models for the study of hair follicles. The journal of investigative dermatology Symposium proceedings / the Society for Investigative Dermatology, Inc [and] European Society for Dermatological Research. 2003; 8:39–45.

Repetto M, Semprine J, Boveris A. Lipid Peroxidation : Chemical Mechanism, Biological Implications and Analytical Determination. Journal of Free Radicals in Biology & Medicine. 2012; 1:3–30.

Rogers, G. The epidermis. New York: Academic Press; 1964. Structural and biochemical features of the hair follicle; p. 179

Rompolas P, Deschene ER, Zito G, Gonzalez DG, Saotome I, Haberman AM, et al. Live imaging of stem cell and progeny behaviour in physiological hair-follicle regeneration. Nature. 2012; 487:496–9. [PubMed: 22763436]

Stenn KS, Paus R. Controls of hair follicle cycling. Physiological reviews. 2001; 81:449–94. [PubMed: 11152763]

Swift, JA. Chemistry of Natural Protein Fibers. Asquith, RS., editor. Boston, MA: Springer US; 1977. p. 81-146.

Van Beek N, Bodó E, Kromminga A, Gáspár E, Meyer K, Zmijewski Ma, et al. Thyroid hormones directly alter human hair follicle functions: Anagen prolongation and stimulation of both hair matrix keratinocyte proliferation and hair pigmentation. Journal of Clinical Endocrinology and Metabolism. 2008; 93:4381–8. [PubMed: 18728176]

Vidali S, Chéret J, Giesen M, Haeger S, Alam M, Watson REB, et al. Thyroid hormones enhance mitochondrial function in human epidermis. Journal of Investigative Dermatology. 2016:1–10. [PubMed: 26763413]

Vidali S, Knuever J, Lerchner J, Giesen M, Bíró T, Klinger M, et al. Hypothalamic–Pituitary– Thyroid Axis Hormones Stimulate Mitochondrial Function and Biogenesis in Human Hair Follicles. Journal of Investigative Dermatology. 2014; 134:33–42. [PubMed: 23949722]

Williams R, Philpott MP, Kealey T. Metabolism of freshly isolated human hair follicles capable of hair elongation: a glutaminolytic, aerobic glycolytic tissue. J Invest Dermatol. 1993; 100:834–40. [PubMed: 8496624]

Zahrebelski G, Nieminen A, al-Ghoul K, Qian T, Herman B, Lemasters J. Progression of subcellular changes during chemical hypoxia to cultured rat hepatocytes: a laser scanning confocal microscopic study. Hepatology. 1995; 21:1361–72. [PubMed: 7737643]

Abbreviations

ΔΨ	mitochondrial membrane potential
PI	propidium iodide
Rh123	rhodamine 123
ROS	reactive oxygen species

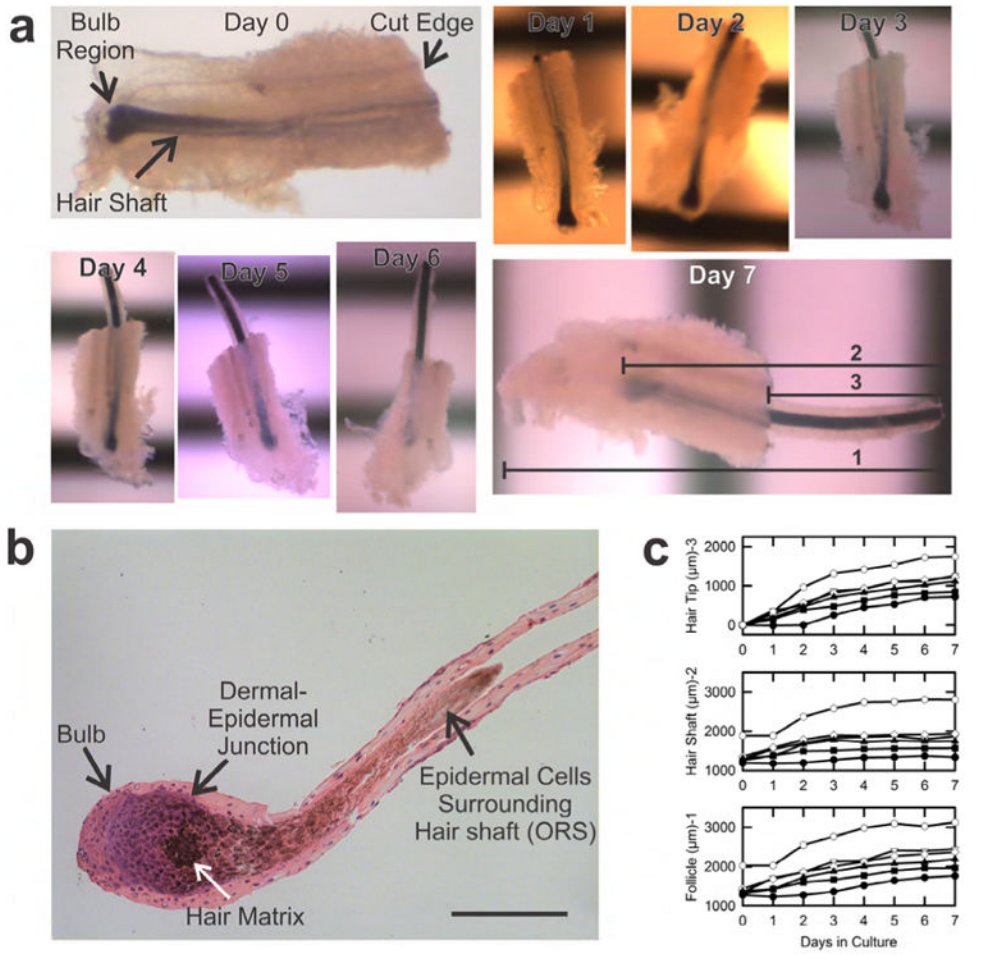

Fig. 1. Isolated, dissected bovine hair follicles in culture

A. Shown are micrographs of a growing follicle during 7 days in culture. As illustrated for Day 7 of culture, hair growth was indicated by increases of the total length of the follicle (1), the length of the hair shaft (2), and the length of hair shaft protruding beyond the cut distal edge of the follicle (3). Horizontal black stripes are a millimeter ruler. **B.** H&E staining of a typical isolated bovine follicle. Scale bar in Panel b is 200 μ. **C.** Growth of six follicles dissected from a single cow skin.

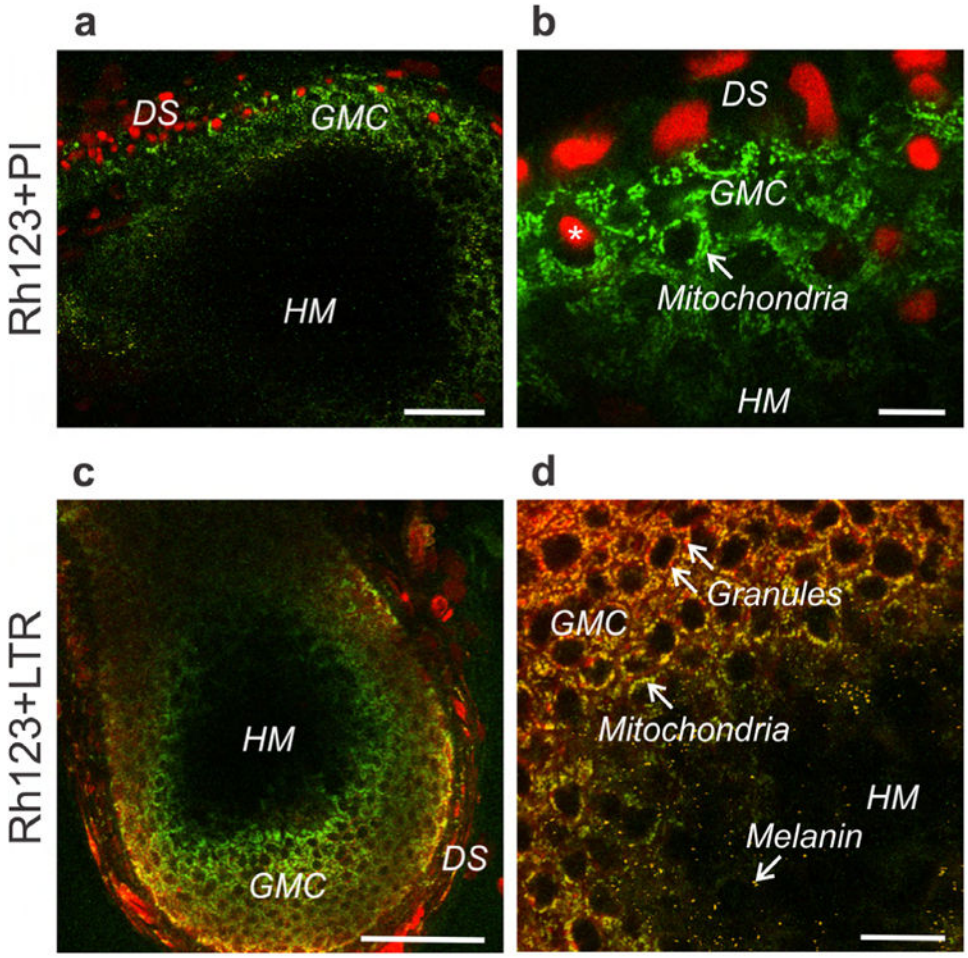

Fig. 2. Multiphoton imaging of cell viability, mitochondrial polarization and secretory vesicles in growing bovine hair follicles

A,B. Bovine hair follicle loaded with green-fluorescing Rh123 and red-fluorescing PI and imaged by muliphoton microscopy. **A** scale bar = 50 μm. **B** scale bar = 25 μm. *, nonviable cell nuclei labeled with PI. **C,D**. A bovine hair follicle visualized with LTR (red, secretory vesicles) and Rh123 (green, mitochondrial ΔΨ). DS, dermal sheath; GMC, germative matrix cells; HM, hair matrix. **C.** scale bar =100 μm. **D.** scale bar = 25 μm.

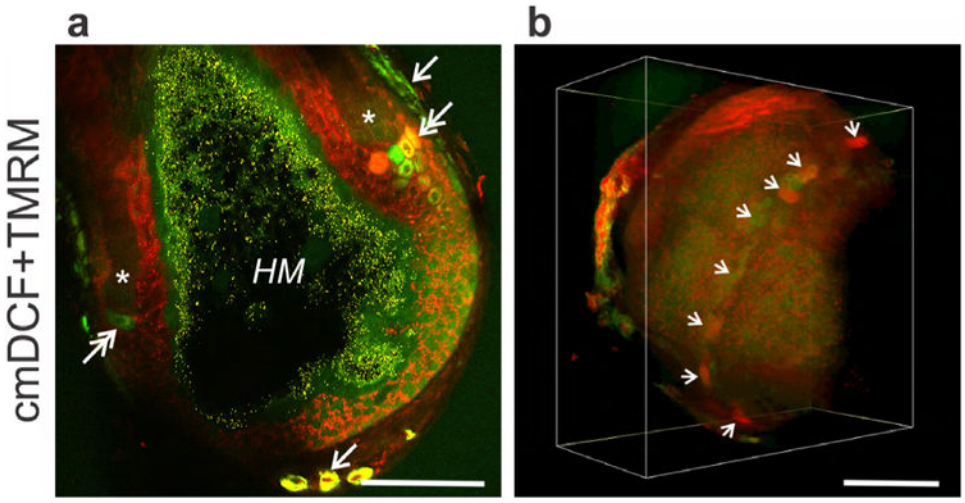

Fig. 3. Formation of reactive oxygen species in growing bovine hair follicles

A. Bovine hair follicle visualized with TMRM (red, $\Delta\Psi$) and cmH_2DCF-DA (green, ROS). Arrows identify dermal sheath cells labeled with cmDCF for ROS. Double arrows identify clusters of cells with high cmDCF and/or TMRM fluorescence at the apex of clefts (*) of mitochondrial depolarization (loss of red TMRM fluorescence). Yellow granules in black areas are melanin inside the hair matrix (HM). **B.** Three-dimensional projection of cmDCF and TMRM fluorescence. Arrows identify cells with high cmDCF and/or TMRM fluorescence. In both **A.** and **B.** scale bar = 100 μm.

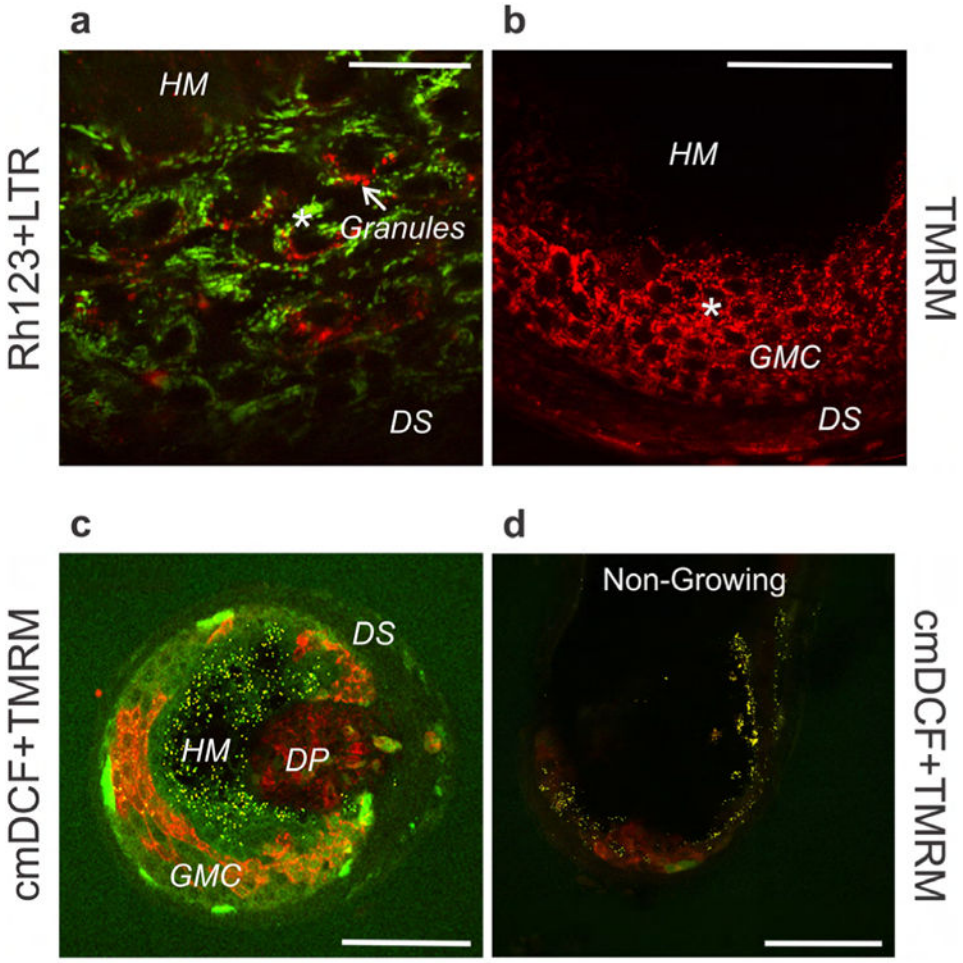

Fig. 4. Mitochondrial hyperpolarization, degranulation and formation of reactive oxygen species in growing and non-growing bovine hair follicles

A,B. Dissected bovine hair follicles visualized with Rh123 (green, ΔΨ) plus LTR (red, secretory vesicles) (**A**) or TMRM (red, ΔΨ). Scale bar = 25 μm (**B**). *, hyperpolarized mitochondria. Scale bar = 50 μm. **C.** Bovine hair follicle loaded with cmDCF (green, ROS) and TMRM (red, ΔΨ) and cross-sectionally imaged 100 μm distal from its base. Scale bar =100 μm. **D.** cmDCF- and TMRM-loaded non-growing bovine hair follicle imaged from the side at 60 μm from the surface. DP, dermal papilla; DS, dermal sheath; GMC, germative matrix cells; HM, hair matrix. Scale bar = 100 μm.

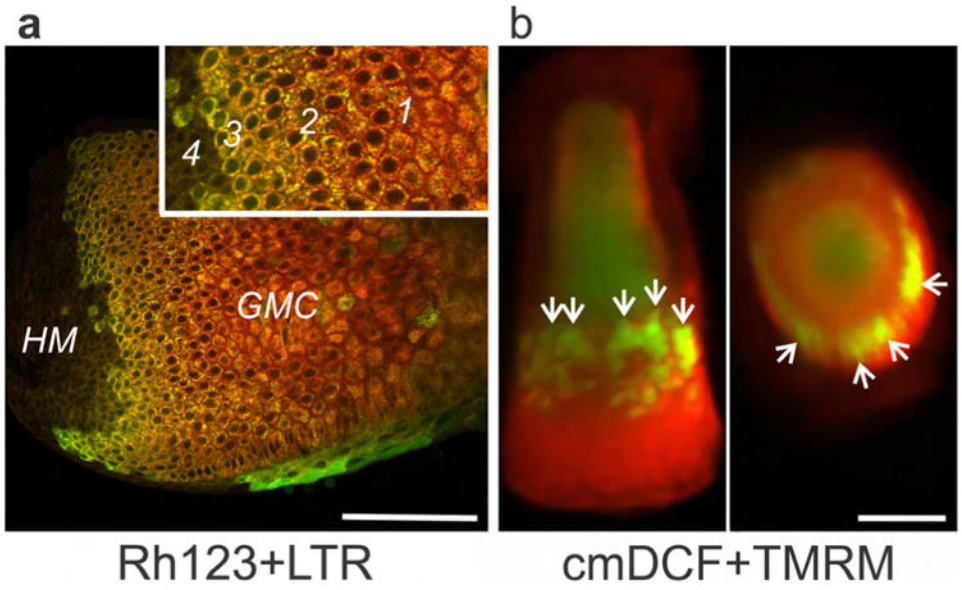

Fig. 5. Mitochondrial hyperpolarization and degranulation in plucked human hairs

A. Human hair pluck imaged by multiphoton microscopy after loading with Rh123 and LTR. Inset shows areas of LTR-labeled vesicle (granule) formation (*1*), mitochondrial hyperpolarization (*2*), loss of vesicles (*3*), and mitochondrial depolarization (*4*). Scale bar = 100 μm. **B.** Three-dimensional longitudinal projection (left) and latitudinal cross section (right) of a plucked human hair imaged with cmDCF and TMRE (red, $\Delta\Psi$) by light sheet microscopy. Arrows identify hyperpolarized and ROS-generating cells in the 'ring of fire'. Scale bar = 200 μm.

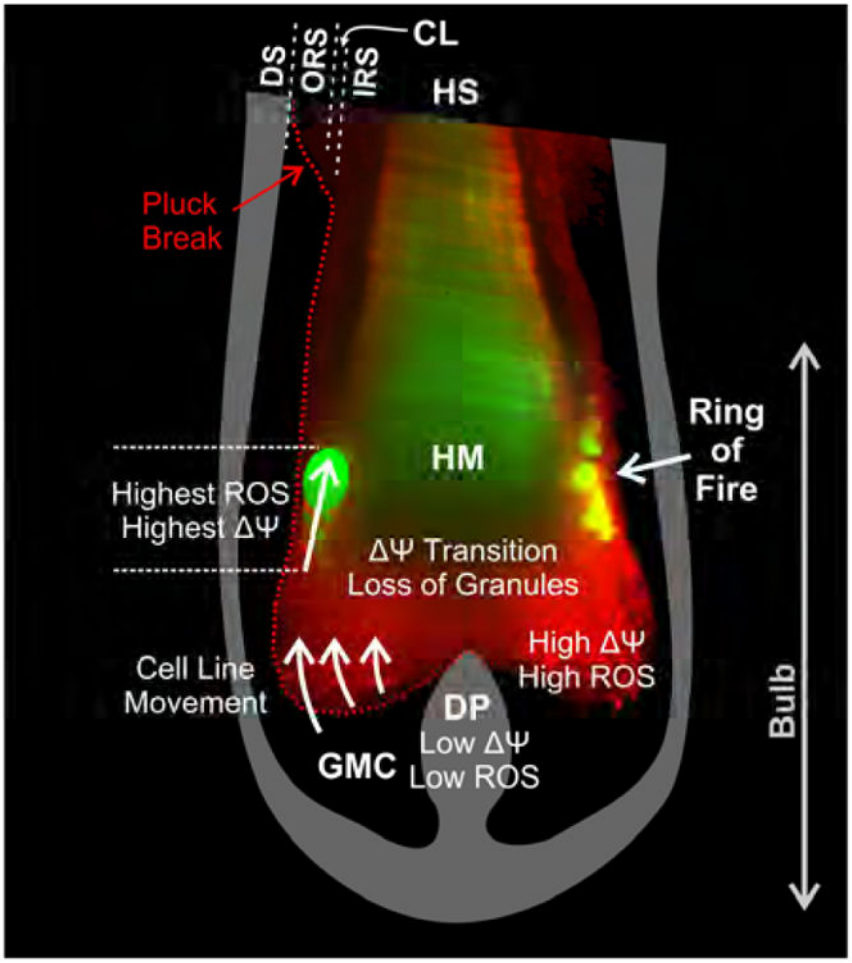

Fig. 6. Scheme of hair follicle metabolism in a longitudinal section of a human follicle

Mitochondrial ΔΨ increases as proliferative germative matrix cells (GMC) move upwards, culminating in a burst of ROS generation, loss of granules, and mitochondrial depolarization. Hyperpolarization and ROS generation are particularly intense in a circumferential 'ring of fire'. Scheme is superimposed on a light-sheet image of a plucked human hair labeled with TMRE and cmH2DCF. DS, dermal sheath; DP, dermal papilla; GMC, germative cell matrix; HM, hair matrix; HS, hair shaft; IRS, inner root sheath; CL, companion layer; ORS, outer root sheath.